THE USE OF HYPERSPECTRAL DATA FOR PRECISION FARMING

K. Staenz, J.-C. Deguise, J.M. Chen, H. McNairn, and R.J. Brown
Canada Centre for Remote Sensing, Ottawa Ontario, Canada

T. Szeredi
MacDonald Dettwiler and Associates, Richmond, British Columbia, Canada

M. McGovern
Agriculture Canada, Ottawa, Ontario, Canada

Commission VII, Working Group I

KEY WORDS: Leaf area index, precision farming, hyperspectral *casi* data cube, surface reflectance, spectral unmixing, crop fraction.

ABSTRACT: A technique is proposed to estimate leaf area index (LAI) using the crop endmember fraction derived with spectral unmixing. 96-band hyperspectral data acquired with the Compact Airborne Spectrographic Imager (*casi*) over two agricultural sites were used to test the approach against measured LAI data and LAI computed with a NDVI-based semi-empirical model. For this purpose, the radiance data were converted to surface reflectance prior to the extraction of the crop fractions which were retrieved with constrained linear unmixing. The preliminary validation tests indicate that the proposed technique has potential to estimate the effective LAI from the crop fraction. This technique has the advantage, compared to other approaches, of separating the crop from unwanted portions of vegetation such as weeds. This should lead to a more accurate estimation of LAI.

1.0 INTRODUCTION

Image-based remote sensing can play a significant role in precision farming (Moran et al., 1997), providing information for crop management on a within-field basis. With the advent of the imaging spectrometer, a fundamental new remotely sensed data set became available for this purpose (Staenz 1992). The high spectral dimensionality of such data enables the extraction of quantitative information never before possible with broad-band imaging sensors. In particular, hyperspectral data can be used to improve the detection of within-field variability with respect to crop production, to determine the cause of within-field spatial variability, and to pararmeterize and validate crop models (Moran et al., 1995; Carter, 1994; Maas, 1993).

In this paper, the potential of hyperspectral Compact Airborne Spectrographic Imager (*casi*) data has been evaluated for the detection of spatial variability on a field basis for cash crops near Altona, Manitoba (Canada). Special emphasis was devoted to the extraction of the green leaf area index (LAI). LAI is a fundamental crop parameter that provides a valuable source for crop growth modeling (Moran et al., 1995; Bouman, 1992; Bauer, 1985; Wiegand et al., 1986). Since LAI is functionally related to spectral reflectance, a variety of techniques have been developed using remotely sensed data. Vegetation indices are involved especially for the estimation of LAI (Baret and Guyot, 1991; Wiegand and Richardson, 1990; Clevers, 1989). One of the disadvantages of the use of vegetation indices is the fact that these indices are sensitive to the total amount of vegetation cover within a pixel without distinguishing between crop, weeds, and other vegetation components. A new technique that only takes the crop portion of the vegetation into account for estimating the LAI is presented in this paper.

2.0 DATA ACQUISITION

casi data were acquired over agricultural test sites near Altona and Birtle, Manitoba on July 25, 1996 during maximum vegetation growth. The flat test sites had a variety of cash crops, such as cereal grains, canola, sugar beets, and beans. A typical field size is 400 m by 800 m.

The *casi* data sets were collected in the wavelength range from 458 nm to 1000 nm in 96 contiguous, 6.8 nm wide spectral bands, sampled at 5.8 nm intervals (Anger et al., 1996). In this data acquisition configuration, the swath consists of 304 pixels with a ground resolution of 4 m across and 4 m along track at a flight altitude of 2745 m above sea level.

Ground reference information relevant for this study includes crop type, LAI, and biomass. Biomass samples were collected from 8 to 12, 0.5 m by 0.5 m plots along a diagonal transect of selected fields with sample plots approximately 50 m to 60 m apart. LAI was estimated from the leaf material collected from the biomass sample by dividing the total leaf area by the sample plot (unit) area.

3.0 DATA PREPROCESSING

The preprocessing of *casi* data included the removal of noise, most significant aircraft motion effects, surface reflectance retrieval, and post-processing of the retrieved surface reflectance spectra (Figure 1).

Noise (non-periodic horizontal striping), which especially affects bands at the two extremes of the *casi* wavelength coverage, was removed in the principal component (PC) domain using the last 89 of 96 PC images. The average of each line per PC image was calculated and subsequently plotted against the line number. A Gaussian smoothing with a window of 15 lines was then applied to the data. This enabled the computation of a correction factor (gain) for each line to adjust the original mean values to the smoothed ones. The gain was calculated by dividing the smoothed values by the original line means. In a final step, the entire 96-PC image set was inversely transformed back to the spectral band domain.

In order to correct for the most significant aircraft motion effect, the roll was estimated using the navigation data to calculate lateral pixel shifts for each line. These shifts were then applied to the entire image cube on a line by line basis.

In the next processing stage, surface reflectances were computed from calibrated at-sensor radiance data, compensating for atmospheric absorption and scattering effects. The procedure is based on a look-up table (LUT) approach with tunable breakpoints as described in Staenz and Williams (1997), to reduce significantly the number of radiative transfer (RT) code runs. MODTRAN3 was used in forward mode to generate the radiance LUTs, one of each for a 5% and 60% reflectance. These LUTs were produced for five pixel locations equally spaced across the swath, including nadir and swath edges, for a range of water vapour contents, and for single values of aerosol optical depth (horizontal visibility) and terrain elevation. The specification of these parameters and others required for input into the MODTRAN3 RT code are listed in Table 1. For the retrieval of the surface reflectance from the Altona cube, the LUT radiances were adjusted for the ground target's (pixel) position in the swath and the water vapour content using an n-dimensional bilinear interpolation (Press et al., 1992). For this purpose, the water vapour content was estimated on a per pixel-basis from the image cube with an iterative curve fitting technique (Staenz et al., 1997). For the Birtle data cube, the LUTs were only interpolated for the pixel position since a single water vapour amount was used for the entire cube. The surface reflectance ρ was then calculated for each pixel as follows:

$$\rho = \frac{L - L_a}{A + B + S\left(L - L_a\right)} , \tag{1}$$

where L is the at-sensor radiance provided by the image cube, L_a is the radiance backscattered by the atmosphere, S is the spherical albedo of the atmosphere, and A and B are coefficients that depend on geometric and atmospheric conditions. The unknowns A, B, S, and L_a were calculated from the equations

$$L_{gi} = \frac{\rho_i}{1 - \rho_i S} + L_a , \quad i = 1, 2 \tag{2}$$

and

$$L_{pi} = \frac{\rho_i}{1 - \rho_i S} + L_a , \quad i = 1, 2 \tag{3}$$

where L_{gi} is the at-sensor radiance reflected by the target and L_{pi} is the at-sensor radiance scattered into the path by the surrounding targets, respectively. These equations can be solved on a per pixel basis for each set of (ρ_i , L_{gi} , and L_{pi}) obtained from the LUTs by interpolation for the different geometric and atmospheric conditions. With i = 1 and 2 (ρ_1 = 5%, ρ_2 = 60%), this yields a system of four equations with four unknowns.

In a last step, band-to-band errors due to atmospheric modelling and calibration effects in the retrieved surface reflectance spectra were removed using a Gaussian smoothing with a 80 nm window between 820 nm and 1000 nm. A resulting reflectance spectrum of canola is shown in comparison with non-smoothed data in Figure 2.

Table 1
Input Parameters for MODTRAN3 Code Runs

Test Site	**Altona**	**Birtle**
Atmospheric model	Mid-latitude summer	Mid-latitude summer
Aerosol model	Continental	Continental
Date of overflight	July 25, 1996	July 25, 1996
Solar zenith angle	31.3°	49.7°
Solar azimuth angle	155.9°	109.5°
Sensor zenith angle	Variable	Variable
Sensor azimuth angle	Variable	Variable
Terrain elevation above sea level	0.250 km	0.540 km
Sensor altitude above sea level	2.745 km	3.035 km
Water vapour content	Variable	2.75 g/cm^2
Ozone column	as per model	as per model
CO_2 mixing ratio	as per model	as per model
Horizontal visibility	40 km	30 km

4.0 LAI COMPUTATION

The LAI can be expressed as follows (Chen et al., 1991):

$$LAI = \frac{LAI_e}{\Omega} , \tag{4}$$

where LAI_e is the effective LAI and Ω is the clumping index. Ω varies between 0 and 1 for clumped canopies, but can be larger than 1 for regularly distributed foliage. For most row crops such as beans, Ω is less than 1. For crops with more random plant distribution such as canola, Ω approximates 1. Since Ω is generally unknown, only LAI_e can be calculated according to the following formula (Ross, 1981):

$$LAI_e = \frac{\cos\alpha}{G}\left(-\ln P\right) , \tag{5}$$

where P is the probability of a view line or a beam of radiation at an incident angle α passing through a horizontally uniform plant canopy with random leaf angular and spatial distribution and G is the mean projection coefficient of unit foliage area on a plane perpendicular to α.

In order to estimate LAI_e from hyperspectral data, G can be set to 0.5 for plants with leaf angle randomly distributed such as for agricultural crops (Norman, 1979). The incident angle α corresponds to the sensor viewing zenith angle. In our case, α was set to 0° (nadir looking), which was appropriate for the viewing angles under consideration ($\leq$15°). P represents the gap fraction, which was determined by spectral unmixing as follows:

$$P = 1 - f_c , \tag{6}$$

where f_c is the fraction of the crop endmember. LAI_e can then be expressed from hyperspectral data according to equations (5) and (6) by

$$LAI_e = -2\ln\left(1-f_c\right). \qquad (7)$$

In order to retrieve f_c, a constrained linear unmixing procedure was applied to the image (reflectance) cube to map the different field components represented by the endmembers of crop, weeds, and soil. These endmembers were selected from the cube itself. A principal component (PC) analysis was then performed on the cube and scatter plots of a pair of PCs were generated. The endmembers were selected from averages of those pixels located in the extremities of the scatter plot. These pixels are often referred to as the "purest pixels" (Boardman, 1993).

The retrieved endmembers were then used in unmixing, which expresses the reflectance spectrum of an image pixel as a linear sum of N endmember spectra as follows (Shimabukuru and Smith, 1991; Boardman, 1995):

$$\rho_k^{(x,y)} = \sum_{e=1}^{N} f_e^{(x,y)} S_{ek}, \; k = 1,2, \ldots\ldots, M \qquad (8)$$

where $\rho_k^{(x,y)}$ is the reflectance in band k of the spectrum for pixel (x, y), S_{ek} is the reflectance in band k of the e^{th} endmember spectrum, $f_e^{(x,y)}$ is the fraction of endmember e contributing to the spectrum of pixel (x, y), and M is the total number of bands in the spectrum. In constrained unmixing, the fractions are positive and the sum of the fractions for pixel (x, y) equals 1.

An overview of the data processing layout for computing the effective LAI is presented in Figure 3.

5.0 RESULTS

Validation of the estimated LAI was performed for the three crop types of bean, canola, and wheat, each with a distinct plant architecture. The estimated LAI values were compared against those derived from direct measurements and those calculated with a semi-empirical approach using the normalized difference vegetation index (NDVI) as a function of surface reflectance using *casi* bands 36 (659 nm) and 63 (813 nm).

5.1 Comparison With Ground-based Measurements

Due to the uncertainty of locating the biomass sample plots in the imagery, a 3 by 3 pixel average of the crop fractions corresponding to the sample plot areas was used to compute the LAI with equation (7). Subsequently, the results were compared to the LAI derived from the biomass samples (Figure 4). The root mean square deviation from the x=y line is 0.9. These validation results indicate that the LAI based on the image fraction provides an absolute measure of the LAI accurate to within 0.9, two thirds of the time. Some of the deviation can be related to the difficulties of locating the sample plots in the imagery. An accurate location of the sample plot is important since the fractions can vary up to 30% within the selected 3 by 3 pixel window.

Table 2 indicates that the LAI_e of beans was smaller than the measured LAI on average. This is probably due to the foliage clumping as a result of the distinct row structure. For the other two crops without open row struture $\Omega \sim 1$, therefore LAI_e should be approximately equal to LAI. The estimated LAI_e of canola agrees quite well on average with the measured LAI, but the LAI_e of wheat was overestimated. It is possible that the wheat foliage was more regularly distributed than random.

Table 2.
Comparison of leaf area index determined from the image fraction (LAI_e) and direct measurements (LAI) for different crop types. LAI_e and LAI represent the mean of the sample plots per field; s is the standard deviation, and n is the number of sample plots.

Field	n	$LAI_e \pm s$	$LAI \pm s$
Bean	10	2.38 ± 0.72	2.68 ± 1.25
Canola	5	3.06 ± 0.68	3.02 ± 0.86
Wheat	9	1.76 ± 0.81	1.38 ± 0.60

5.2 Comparison with LAI Calculated from NDVI

Additional validation tests were carried out comparing the LAI values calculated from the crop fraction with those derived from NDVI. The following relationship was used to compute the LAI for the different crop types (Baret and Guyot, 1991):

$$LAI_e\,(NDVI) = -\frac{1}{k}\ln\left(\frac{NDVI - NDVI_M}{NDVI_S - NDVI_M}\right), \qquad (9)$$

where $NDVI_M$ is the maximum value of NDVI found in the image (asymptotic value of NDVI when LAI_e tends towards infinity), $NDVI_S$ is the NDVI of soil retrieved from the site under consideration in the imagery, and k is the coefficient which controls the slope of the relationship. The parameters to calculate LAI_e (NDVI) are listed in Table 3. Equation (7) was used to calculate the $LAI_e\,(f_c)$ from the image fraction. The fraction f_c includes in this case the crop as well as the other vegetative fractions such as weeds since NDVI represents a value for the total vegetation cover. k in equation (9) was selected such that

$$LAI_e\,(NDVI) = LAI_e\left(f_c\right)\,\left[1 \pm s\right], \qquad (10)$$

where s is the standard deviation of LAI_e. The results as shown in Table 3 for the different crop types indicate that values of LAI_e (NDVI) and $LAI_e\,(f_c)$ are within a standard deviation of about 0.3 for beans and wheat and 0.2 for canola.

Table 3
Standard deviation (s) of the computed $LAI_e\,(f_c)$ with respect to the LAI(NDVI) estimated from NDVI. Parameters required to calculate the NDVI based LAI are also listed. ($NDVI_M$ = maximum value of NDVI found in the image, $NDVI_S$ = NDVI value of soil retrieved from the image, k = coefficient which controls the relationship as stated in equation (9)).

Field	$NDVI_M$	$NDVI_S$	k	s
Beans	0.97	0.22	0.52	0.29
Canola	0.97	0.22	0.55	0.21
Wheat	0.96	0.31	0.83	0.30

6.0 CONCLUSIONS

Preliminary validation tests indicate that using linear spectral unmixing to extract the crop endmember (gap) fraction has potential for the estimation of the effective LAI. Results for bean, canola, and wheat showed a reasonable agreement with LAI derived from direct measurements considering the uncertainty in foliage distribution patterns (clumped, random, or regularly) and in locating the sample plots in the imagery. A comparison with LAI values calculated with a semi-empirical approach using NDVI and those estimated from the image fraction indicate that the two values agree within a standard deviation of at most 0.3. The proposed technique has the advantage that crop specific fractions can be determined and, therefore, unwanted portions of vegetation such as weeds can be excluded. This is not the case for LAI estimations based on vegetation indices such as NDVI.

7.0 ACKNOWLEDGEMENT

The authors thank C. Burke for word-processing of this paper.

8.0 REFERENCES

Anger, C.D., S. Achal, T. Ivanco, S.Mah, R. Price, and J. Busler, 1996. Extended Operational Capabilities of *casi*. Proceedings of the Second International Airborne Remote Sensing Conference, San Francisco, California, pp.124-133.

Baret, F., and G. Guyot, 1991. Potentials and Limits of Vegetation Indices for LAI and APAR Assessment. Remote Sensing of the Environment, 35:161-173.

Bauer, M.E., 1985. Spectral Inputs to Crop Identification and Condition Assessment. Proc. IEEE, 73:1071-1085.

Bouman, B.A.M., 1992. Linking Physical Remote Sensing Models with Crop Growth Simulation Models, Appliced for Sugar Beet. International Journal of Remote Sensing, 13:2565-2581.

Boardman, J.W., 1993. Automating Spectra Unmixing of AVIRIS Data Using Convex Geometric Concepts. Summaries of the Fourth Annual JPL Airborne Geoscience Workshop, JPL Publication 93-26, Pasadena, California, Vol.1, pp.11-14.

Boardman, J.W., 1995. Analysis, Understanding and Visualization of Hyperspectral Data Convex Sets in N-Space. Proceedings of SPIE's International Conference on Imaging Spectrometry, Orlanda, Florida, Vol. 2480, pp.14-20.

Carter, G.A., 1994. Ratios of Leaf Reflectances in Narrow Wavebands as Indicators of Plant Stress. International Journal of Remote Sensing, 15:697-703.

Chen, J.M., T.A. Black, and R.S. Adams, 1991. Evaluation of Hemispherical Photography for Determining Plant Area Index and Geometry of a Forest Stand. Agriculture and Forest Meteorology, 56:129-143.

Clevers, J.G.P.W., 1989. The Application of a Weighed Infra-Red Vegetation Index by Correcting for Soil Moisture. Remote Sensing of Environment, 29:25-37.

Maas, S.J., 1993. Parameterized Model of Gramineous Crop Growth: II. Within-Season Simulation Calibration. Agronomy Journal, 85:354-358.

Moran, M.S., S.J. Maas, and P.J. Pinter, 1995. Combining Remote Sensing and Modeling for Estimating Surface Evapotranspiration and Biomass Production. Remote Sensing Reviews, 12:335-353.

Moran, M.S., Y. Inoue, and E.M. Barnes, 1997. Opportunities and Limitations for Image-Based Remote Sensing in Precision Crop Management. Remote Sensing of Environment, 61:319-346.

Norman, J.M., 1979. Modelling the Complete Crop Canopy. In: B.J. Barfield and J.F. Gerber (Editors), Modification of the Aerial Environment of Plants. American Society of Agricultural Engineers, St. Joseph, Michigan, pp.249-277.

Press, W.H., S.A. Teukolsky, W.T. Vetterling, and B.P. Flannery, 1992. Numerical Recipes in C. Cambridge University Press, Cambridge, England, pp.123-125.

Ross, J., 1981. The Radiation Regime and Architecture of Plant Stands. Dr. W. Junk Publishers.

Shimabukuru, Y.E., and J.A. Smith, 1991. The Least Squares Mixing Models to Generate Fraction Images From Remote Sensing on Multispectral Data. IEEE Transactions on Geoscience and Remote Sensing, 29:16-20.

Staenz, K., 1992. A Decade of Imaging Spectrometry in Canada. Canadian Journal of Remote Sensing, 18(40:187-1997.

Staenz, K., and D.J. Williams, 1997. Retrieval of Surface Reflectance from Hyperspectral Data Using a Look-Up Table Approach. Canadian Journal of Remote Sensing, 23(4):354-368.

Staenz, K., T. Szeredi, R.J. Brown, H. McNairn, and R. VanAcker, 1997. Hyperspectral Information Extraction Techniques Applied to Agricultural *casi* Data for Detection of Within-Field Variations. Proceedings of the International Symposium in the Era of Radarsat and the Nineteenth Canadian Symposium on Remote Sensing, Ottawa, Ontario, Canada, 8 pages (CD-ROM).

Wiegand, C.L., A.J. Richardson, and R.J. Nixon, 1986. Spectral Component Analysis: A Bridge Between Spectral Observations and Agrometeorological Crop Models. IEEE Transactions on Geoscience and Remote Sensing, GE-24:83-88.

Wiegand, C.L., and A.J. Richardson, 1990. Use of Spectral Vegetation Indices to Infer leaf Area, Transpiration and Yield: I. Rationale. Agronomy Journal, 82(3): G23-G29.

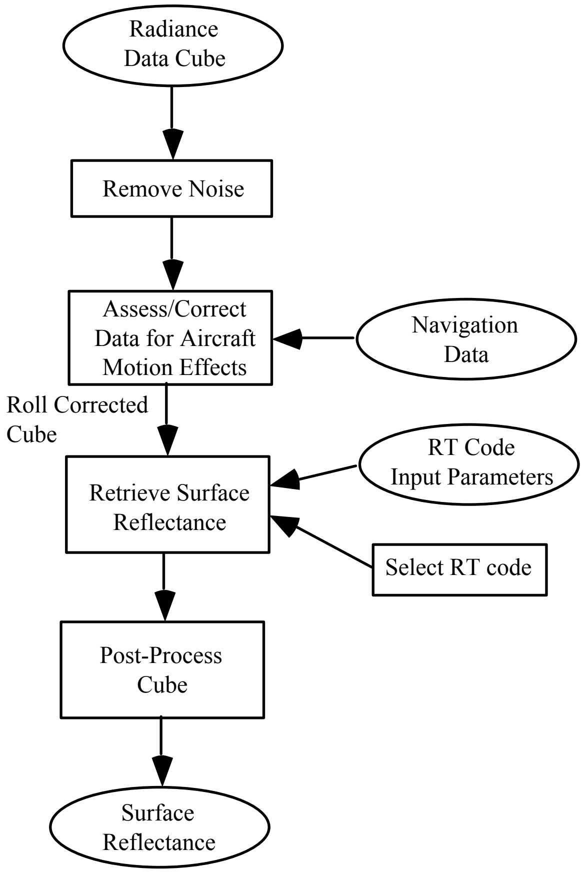

Figure 1: Data pre-processing flow.

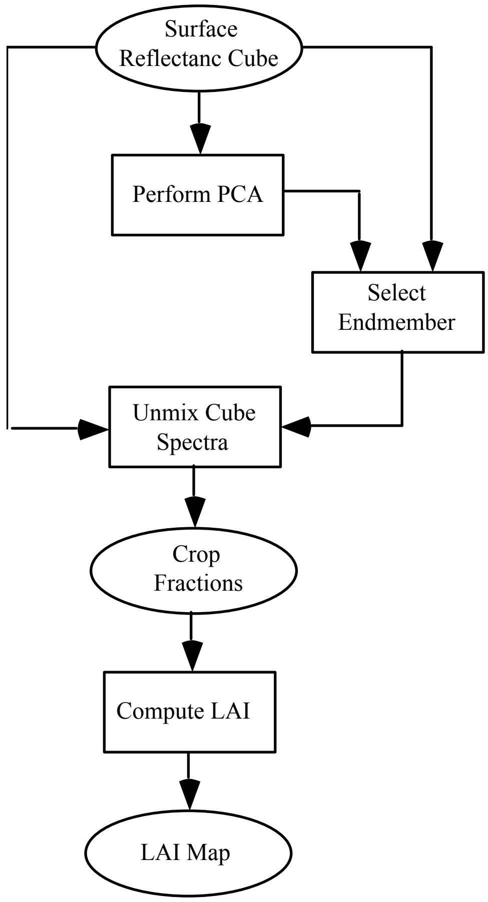

Figure 3: Data processing layout for leaf area index (LAI) computation.

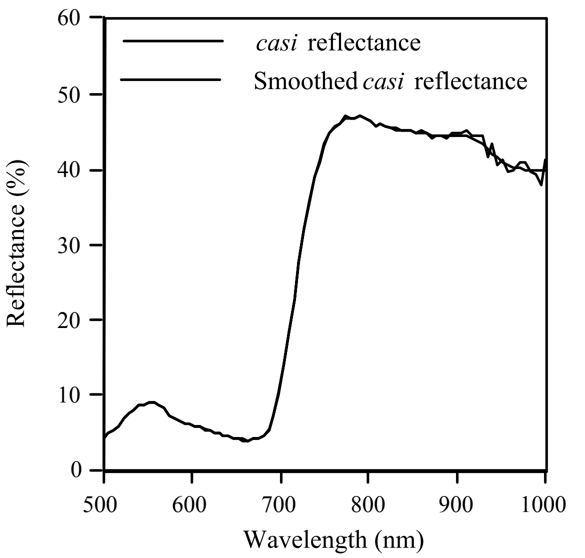

Figure 2: *casi* surface reflectance of canola. The *casi* spectrum was averaged over four adjacent pixels.

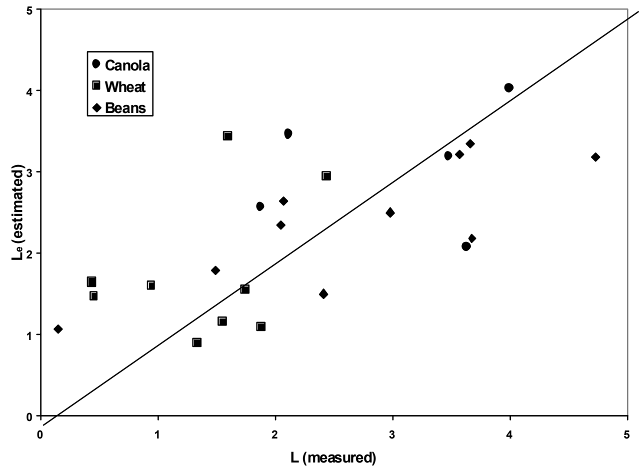

Figure 4: Relationship between the LAI derived from direct measurements L (measured) and from the image cube L_e (image). The solid line represents the x=y line.